NeuroImage 291 (2024) 120588

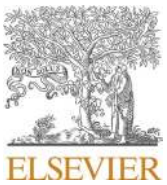

Contents lists available at ScienceDirect

NeuroImage

journal homepage: www.elsevier.com/locate/ynimg

PENCIL imaging: A novel approach for neuromelanin sensitive MRI in Parkinson's disease

Peng Liu [a,1], Xinhui Wang [a,1], Youmin Zhang [a], Pei Huang [b], Zhijia Jin [a], Zenghui Cheng [a], Yongsheng Chen [c], Qiuyun Xu [d], Kiarash Ghassaban [d], Yu Liu [a], Shengdi Chen [b], Naying He [a,*], Fuhua Yan [a,f,*], E. Mark Haacke [a,c,e,*]

[a] Department of Radiology, Ruijin Hospital, Shanghai Jiao Tong University School of Medicine, No. 197 Ruijin Er Road, Shanghai 200025, China
[b] Department of Neurology, Ruijin Hospital, Shanghai Jiao Tong University School of Medicine, No. 197 Ruijin Er Road, Shanghai 200025, China
[c] Department of Neurology, Wayne State University School of Medicine, 4201St. Antoine, Detroit, MI 48201, USA
[d] SpinTech MRI, Bingham Farms, MI 48025, USA
[e] Department of Radiology, Wayne State University School of Medicine, 3990 John R Street, MRI Concourse, Detroit, MI 48201, USA
[f] Faculty of Medical Imaging Technology, College of Health Science and Technology, Shanghai Jiao Tong University School of Medicine, Shanghai 200025, China

ARTICLE INFO

Keywords:
STAGE imaging
Parkinson's disease
Neuromelanin
Magnetization transfer contrast
Proton density mapping

ABSTRACT

Background: Parkinson's disease (PD) is associated with the loss of neuromelanin (NM) and increased iron in the substantia nigra (SN). Magnetization transfer contrast (MTC) is widely used for NM visualization but has limitations in brain coverage and scan time. This study aimed to develop a new approach called Proton-density Enhanced Neuromelanin Contrast in Low flip angle gradient echo (PENCIL) imaging to visualize NM in the SN.
Methods: This study included 30 PD subjects and 50 healthy controls (HCs) scanned at 3T. PENCIL and MTC images were acquired. NM volume in the SN pars compacta (SNpc), normalized image contrast (Cnorm), and contrast-to-noise ratio (CNR) were calculated. The change of NM volume in the SNpc with age was analyzed using the HC data. A group analysis compared differences between PD subjects and HCs. Receiver operating characteristic (ROC) analysis and area under the curve (AUC) calculations were used to evaluate the diagnostic performance of NM volume and CNR in the SNpc.
Results: PENCIL provided similar visualization and structural information of NM compared to MTC. In HCs, PENCIL showed higher NM volume in the SNpc than MTC, but this difference was not observed in PD subjects. PENCIL had higher CNR, while MTC had higher Cnorm. Both methods revealed a similar pattern of NM volume in SNpc changes with age. There were no significant differences in AUCs between NM volume in SNpc measured by PENCIL and MTC. Both methods exhibited comparable diagnostic performance in this regard.
Conclusions: PENCIL imaging provided improved CNR compared to MTC and showed similar diagnostic performance for differentiating PD subjects from HCs. The major advantage is PENCIL has rapid whole-brain coverage and, when using STAGE imaging, offers a one-stop quantitative assessment of tissue properties.

1. Introduction

Parkinson's disease (PD) is a progressive neurodegenerative disorder characterized by the impairment of voluntary motor control. Its prevalence increases with age (Lotankar et al., 2017). At present, the clinical diagnosis of early PD remains challenging especially when compared to atypical parkinsonian disorders due to its heterogeneous symptoms and variable progression rate. Motor symptoms become apparent when approximately 50–70 % of the neuromelanin (NM) in the substantia nigra pars compacta (SNpc) has depigmented (Damier, 1999). NM is a chelating agent which is believed to play a crucial role in protecting the dopaminergic neurons by binding toxic metals (Oshima et al., 2021). Numerous papers have indicated that the loss of NM volume and increased iron content in the SNpc could serve as imaging biomarkers in PD patients (Ghassaban et al., 2019; Takahashi et al., 2018; Fabbri et al., 2017; Wang et al., 2018b; Prasad et al., 2018; Biondetti et al., 2020;

* Corresponding authors at: No.197 Ruijin Er Road, Shanghai 200025, China.
E-mail addresses: i@nayinghe.com (N. He), yfh11655@rjh.com.cn (F. Yan), nmrimaging@aol.com (E.M. Haacke).
[1] These authors contributed equally to this work.

https://doi.org/10.1016/j.neuroimage.2024.120588
Received 31 August 2023; Received in revised form 11 March 2024; Accepted 25 March 2024
Available online 26 March 2024

Gaurav et al., 2021).

The early implementation of NM sensitive magnetic resonance imaging (NM-MRI) used a fat suppressed 2D T1-weighted (T1W) turbo spin echo (TSE) sequence to highlight the NM in the SN (Sasaki et al., 2006). Another form of NM-MRI uses an off-resonance magnetization transfer contrast (MTC) pulse with a 3D gradient echo (GRE) sequence which allows for whole brain coverage, higher through plane resolution and faster imaging (Nakane et al., 2008). More recent studies have employed multi-echo GRE sequences to simultaneously visualize NM and iron in the SN (Liu et al., 2020; He et al., 2021). However, these imaging methods may require relatively long scan times to obtain sufficient image quality and this can lead to motion artifacts for patients with movement disorders.

When an MTC pulse is used in a low flip angle (FA) 3D GRE sequence where the FA is lower than the Ernst angle for all tissues, the resulting images exhibit spin density characteristics. However, if the FA is close to but larger than the Ernst angle of the cerebral spinal fluid (CSF), the CSF will become darker than the white matter and gray matter, both of which still retain their spin density contrast due to their shorter T1 values relative to the CSF. In contrast, when a high FA is used, as is common in NM-sensitive MRI methods, the T1W nature of the scan suppresses the CSF signal and increases the signal from the white matter. This offsets, in part, the signal loss in the white matter caused by the MTC pulse, resulting in a diminished spin density-like contrast between white matter and gray matter compared to the low FA image. Nevertheless, the MTC pulse suppression is stronger than the increase in signal caused by the lower T1 of each tissue at these FA's. Despite this weakness, the T1W approach has been commonly used as it is believed to facilitate the visualization of NM (Sasaki et al., 2006; Nakane et al., 2008). Practically, the advantage of the high FA MTC approach is the subsequent suppression of the CSF due to the increased T1 weighting, whereas the low FA approach benefits from increased contrast since the white matter has a significantly lower spin density than gray matter or CSF. Recent research has revealed that the visualization of the NM territory in NM-MTC MRI is an indirect measure of the presence of NM in the dopaminergic neurons which have high water content (Watanabe et al., 2019; Trujillo et al., 2017a).

Therefore, our hypothesis is that NM contrast can be obtained from a proton-density-weighted low FA GRE sequence because of its higher water content relative to the surrounding tissues. If successful, this approach would eliminate the need for an MTC pulse and reduce scanning time. In this work, we propose a novel NM-MRI method utilizing STAGE (strategically acquired gradient echo) imaging (Chen et al., 2018; Wang et al., 2018; Haacke et al., 2020). We refer to this low FA approach as PENCIL (Proton density Enhanced Neuromelanin Content Imaging using Low FA gradient echo) imaging. The objective of this study was to optimize the imaging parameters to collect STAGE data and evaluate the resulting contrasts for both healthy controls (HCs) and PD subjects to determine if PENCIL imaging could serve as an alternative to MTC for NM visualization.

2. Materials and methods

2.1. Subjects

This prospective study was approved by the local ethics committee and all participants provided written informed consent. A total of 50 HCs (10 for each decade between 30 and 79 years to map out changes in NM with age) and 30 PD patients were recruited at Ruijin Hospital. Data were obtained from September 2021 to February 2023. The diagnosis of PD and severity of motor symptoms were assessed by two neurologists based, respectively, on the Movement Disorder Society PD Criteria (Postuma et al., 2015) and the Hoehn & Yahr (H&Y) stage along with the MDS Unified Parkinson's Disease Rating Scale Part-III (UPDRS-III) (Goetz et al., 2008). The exclusion criteria for PD subjects included: (1) a history of cerebrovascular disease, brain tumor, head trauma or any type of psychiatric disorder; (2) a Mini-Mental State Examination (MMSE) score less than 24; (3) a history of medication known to cause parkinsonism or affect clinical assessment; and (4) any contraindications to an MRI examination. The inclusion criteria for the HCs included: (1) no family or personal history of PD; (2) no neurological or psychiatric disease; (3) no vascular disease; and (4) no MRI contraindications.

2.2. Data collection

All subjects were scanned on a 3T PRISMA (Siemens, Germany) with a 64-channel head coil using a strategically acquired gradient echo (STAGE) imaging protocol and an MTC sequence. The STAGE imaging parameters were as follows: voxel size = $0.67 \times 1 \times 1.34$ mm^3 (reconstructed to $0.67 \times 0.67 \times 1.34$ mm^3); two different FA scans with an FA = 3° collected twice and an FA = 20° collected once for each participant; TE = 7.5 ms; TR = 17 ms; sampling bandwidth = 100 Hz/pixel; acquisition matrix size = 384×192; number of slices = 120; and a parallel imaging acceleration factor of 2. With both phase and partition encoding using 7/8 partial Fourier and elliptical sampling, the resulting scan time was 3 min for each acquisition, leading to a total scan time of 9 min for whole brain coverage inclusive of two 3° scans and one 20° scan. (A theoretical background for the choice of 3° and 20° is given in the Supplementary Material.) In addition, for comparison purposes, a conventional MTC sequence was acquired twice for each participant as described in previous studies (Liu et al., 2020; He et al., 2023) using a 3D GRE sequence with an MT pulse added (1.2k Hz off-resonance, 500 nominal flip angle, and a pulse duration of 10 ms). The same spatial resolution was used as in the STAGE acquisition along with the following modified imaging parameters: FA = 15°; TE = 7.5 ms; TR = 62 ms; pixel bandwidth = 180 Hz/pixel; number of slices = 48; and a scanning time = 4 min and 31 s for midbrain coverage in one scan. The images were collected parallel to the anterior commissure-posterior commissure (AC/PC) line.

2.3. Data processing

The images from the HCs and PD subjects obtained using the PENCIL and MTC protocols were warped into Montreal Neurological Institute (MNI) space using SPM12 software (Wellcome Department of Imaging Neuroscience, University College London, United Kingdom) implemented in MATLAB 2016b (Mathworks, Natick, MA) creating spatially normalized images. This approach was implemented to provide a template from which we could visually evaluate the differences between the two methods as a collection of data from all subjects.

2.3.1. NM region analysis

The two FA=3° images as well as the two MTC images were averaged to improve the SNR for each method. The averaged images were thereafter referred to as the PENCIL image and MTC image. The regions-of-interest (ROIs) for NM in the SN territory were outlined on both PENCIL and MTC images. All initial boundaries were obtained using the template mapping approach published recently (Jin et al., 2022; Jokar et al., 2023). These boundaries were fine-tuned by two experienced radiologists. This semi-automated approach allowed for human interaction to make the results more accurate. In order to draw the boundaries more accurately, all images were zoomed by a factor of four. The NM boundaries were drawn on five consecutive caudal slices showing the NM and total NM volume was obtained by adding the NM volume over both sides of the SNpcs (Supplementary Fig. 2 second row). The NM volume in the SNpc from different age groups was analyzed for both the PENCIL and MTC approaches.

2.3.2. Contrast analysis

The ROIs of the NM and the adjacent white matter regions are illustrated in Supplementary Fig. 1 and have been implemented similar to previous methods (Isaias et al., 2016; Wang et al., 2021; Gaurav et al.,

2021). We chose circular ROIs in the NM region and compared the contrast to a region in the cerebral peduncles (CP) using the normalized contrast $C_{norm} = (S_{NM} - S_{cp})/S_{cp}$. Also, the contrast-to-noise ratio (CNR) of the NM relative to the surrounding tissue was calculated via: $CNR = (S_{NM} - S_{cp})/noise$, where S_{NM} and S_{cp} represent the mean signal intensity values of the NM and the CP, respectively. The noise was measured by registering and subtracting either two separate 3° images or two separate 15° MTC images. This process removes all spatial variations due to radiofrequency transmit and receive coil effects. Then the mean and standard deviation were found in the homogeneous region and the standard deviation divided by sqrt (2) was used as the noise.

2.3.3. Statistical analysis

The continuous variables were presented as mean ± standard error of the mean while categorical variables were presented as counts with percentages. The *t*-test was used to assess the differences in C_{norm} and CNR between the two different methods for both HCs and PDs. We also assessed the performance of our new approach on the diagnosis of PD. The receiver operating characteristic curve (ROC), area under the curve (AUC), sensitivity, and specificity were calculated. All statistical analyses were performed using IBM SPSS (Chicago, IL, USA). A p-value < 0.05 for two-sided tests was considered statistically significant.

3. Results

A total of 80 participants were included in the analysis, comprised of 50 healthy controls (age range: 30–79 years with 10 subjects for each decade, 54.8 ± 12 years, 23 male) and 30 patients with PD (age range: 32–75 years, 59.4 ± 9.3 years, 19 male). For the analysis of the diagnosis, the age and gender had been matched. Demographic and clinical characteristics as well as Hoehn and Yahr Scale and UPDRS-III for PD patients are provided in Table 1.

3.1. Comparison between PENCIL and MTC imaging

The intra-class coefficients for intra-observer measurements were 0.92 and 0.90 for PENCIL and MTC in HCs, 0.90 and 0.88 for PENCIL and MTC in PD subjects, respectively. Example individual images from the MTC and PENCIL data for a 48-year-old female HC are shown in Supplementary Fig. 2 while Supplementary Fig. 3 shows all the images after transformation to MNI space. The volume of NM on PENCIL images was significantly larger than that on MTC images for HCs (489.4 ± 70.8 vs. 454.3 ± 62.8, $P = 0.01$) while PENCIL and MTC NM volumes in the SNpc were comparable in PD subjects (303.8 ± 93.0 vs. 298.6 ± 76.0, $P = 0.84$) (Fig. 1a and b). The same trend can be observed in MNI space (Fig. 1g and h). The scatter plots for all subjects' NM volume in the SNpc obtained from the two methods are shown in Supplementary Fig. 4. There is a tighter agreement between PENCIL and MTC volume measurements for the PD subjects compared to the HCs. The normalized contrast C_{norm} between NM and the surrounding CP was significantly higher in MTC than that in PENCIL (0.3 ± 0.06 vs. 0.2 ± 0.03 for HCs, 0.21 ± 0.03 vs. 0.29 ± 0.05 for PD subjects, all $P < 0.01$) (Fig. 1c and d). However, the CNR in PENCIL was significantly higher than that in MTC (38.0 ± 5.3 vs. 31.9 ± 5.6, $P < 0.01$ for HCs, 36.3 ± 6.5 vs. 30.9 ± 7.9 for PD subjects, $P = 0.02$) (Fig. 1e and f).

Table 1
Demographic and clinical characteristics of participants.

	Healthy controls	PD patients	P value
Age, years (mean ± std)	54.8 ± 12	59.4 ± 9.3	0.355
Sex, male/female	23/27	19/11	0.589
Disease duration, months	N/A	37.3 ± 30.0	N/A
Hoehn and Yahr Scale	N/A	2 (1–5)	N/A
UPDRS-III	N/A	19.6 ± 14.4	N/A

UPDRS = Unified Parkinson Disease Rating Scale (UPDRS).

3.2. Relationship between age and NM volume in the SNpc

We assessed the NM volume in the SNpc across the age range (Supplementary Fig. 5). For subjects younger than 50 years of age, the NM volume in the SNpc showed an increasing trend with age and it decreased significantly after 50 years.

3.3. Diagnostic ability of PENCIL

Fig. 2 shows representative images of HCs and PD subjects obtained from PENCIL and MTC. The NM was more clearly delineated in HCs than in PD subjects for both methods. The volume and CNR for NM were significantly higher for HCs than for PD subjects (Table 2). The AUCs for NM volume in the SNpc were 0.943 (95 % confidence interval [CI]: 0.862–0.984) in PENCIL and 0.934 (95 % CI: 0.849–0.979) in MTC. The AUCs for CNR were 0.761 (95 % CI: 0.646–0.854) in PENCIL and 0.526 (95 % CI: 0.405–0.645) in MTC (Fig. 3). There were no significant differences in AUCs for NM volume in the SNpc between PENCIL and MTC ($P = 0.775$), while there were significant differences in AUCs for CNR between PENCIL and MTC ($P = 0.024$). There was no significant correlation between UPDRS-III scores and NM volume or CNR for the SNpc.

4. Discussion

In this study, we proposed a new 3D GRE method referred to as PENCIL imaging to visualize tissue containing NM and demonstrated that it can produce high quality NM images compared to conventional MTC images. We found that the PENCIL data showed equivalent or better visualization of NM compared to MTC data especially in caudal slices (which contain predominantly the SNpc). The NM volumes in SNpc were somewhat larger for PENCIL compared to MTC. C_{norm} was lower for PENCIL but the CNR was higher compared to MTC. For the analysis of age, the NM volume in the SNpc showed an increasing trend with age and then gradually decreased with age after about 50 years in both methods. The NM volume in the SNpc from PENCIL and MTC both had good diagnostic ability with no significant difference between the two methods.

The majority of studies (Schwarz et al., 2017; Keren et al., 2009; Priovoulos et al., 2018) have used 2D TSE/GRE sequences, 3D single-echo GRE sequences and 3D multi-echo GRE sequences for NM-MRI, with or without the addition of an MT preparation pulse. Although MT contrast is influenced by the T1 and T2 shortening effects caused by the melanin-iron complex (Trujillo et al., 2017b, 2019), it has been shown that the dominant contrast comes from the high water content in the NM-containing dopaminergic and serotonergic cells (He et al., 2023). A recent study (Liu et al., 2020) evaluated the signal as a function of flip angle to find the optimal FA for NM contrast in the SN and LC using a multi-echo, 3D GRE sequence with MT preparation. They found that the low FA (smaller than the Ernst angle) spin density weighted image gave the best contrast for the NM in the SNpc. Similarly, our study demonstrated that the SNpc could be visualized clearly using the PENCIL technique. Although PENCIL, as used in our study, had lower resolution than the conventional high in-plane resolution and thick slice MTC approaches. It exhibited a favorable CNR and was able to visualize the NM in SNpc well. Given the fact that we proposed collecting the data with both low and high FAs, using STAGE processing it is possible to predict the signal for any FA which allows for optimization of the LC contrast by choosing the appropriate FA (Liu et al., 2020). Too high a FA makes the LC become isointense with WM while a low FA makes it hard to see against the bright CSF in the 4th ventricle. Increasing the flip angle to 7°, enough to suppress the CSF but keep the LC signal high, appears to give the best LC-tissue contrast (Supplementary Fig. 6).

The observed difference in Cnorm between MTC and PENCIL can be attributed to the fact that the MTC pulse enhances the spin density weighted-like contrast in low flip angle data, resulting in higher Cnorm values. On the other hand, the SNR and, consequently, the CNR was

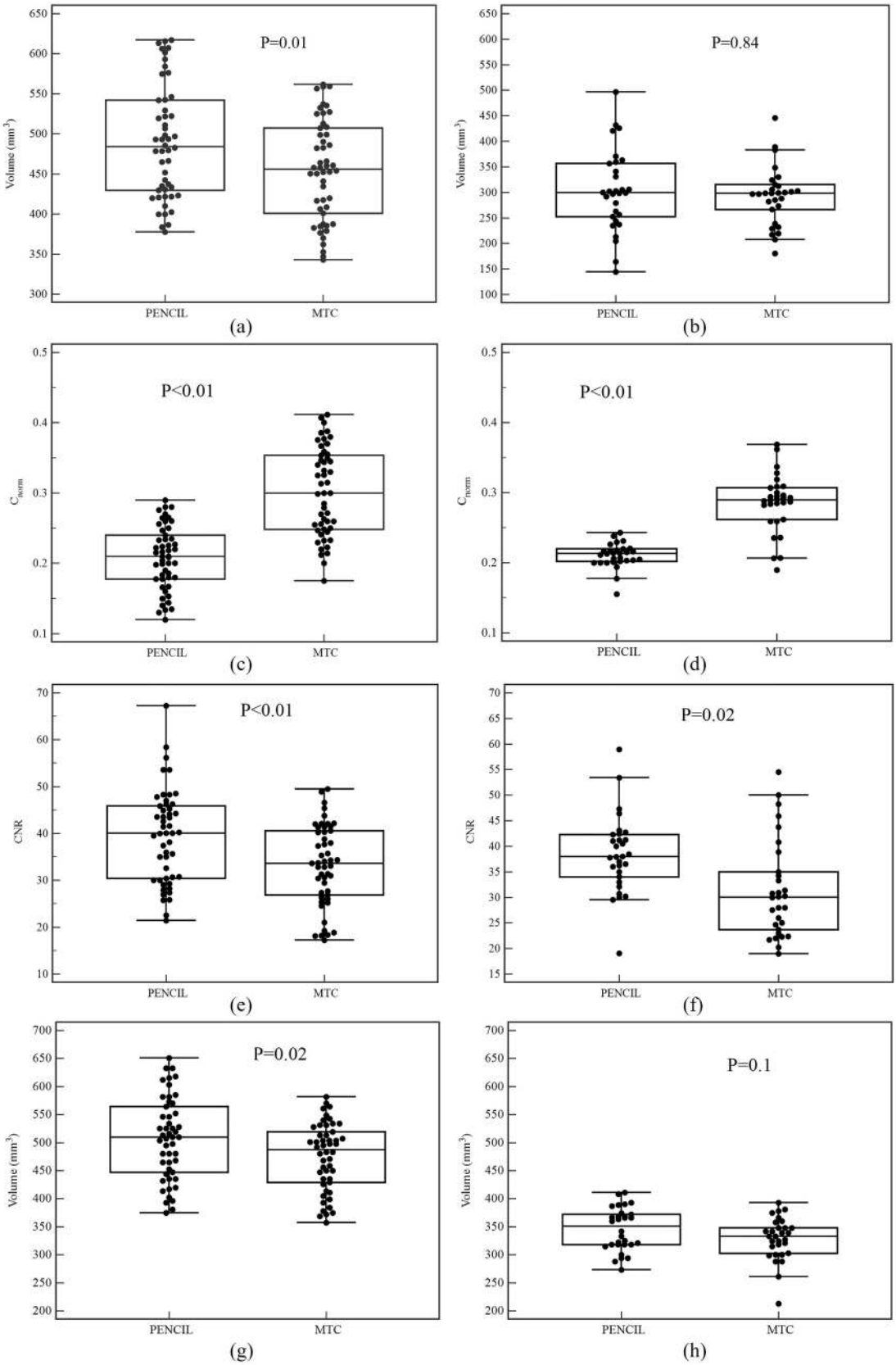

Fig. 1. NM volume in SNpc, normalized contrast ratio C_{norm}, CNR and NM volume in MNI space measured from the PENCIL and MTC data on HC (a, c, e and g) and PD (b, d, f and h). The NM volume was obtained by adding the NM volume over both sides of the SNpcs.

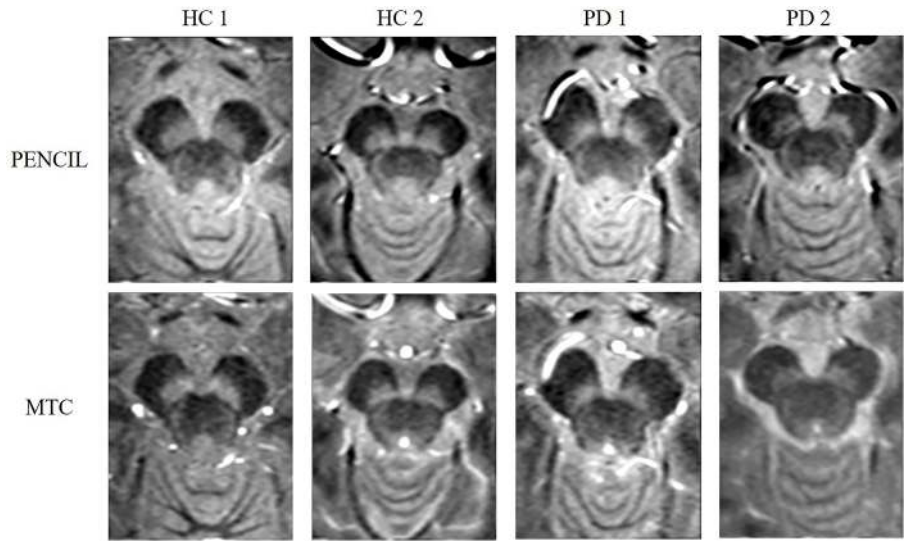

Fig. 2. Representative images of PENCIL and MTC data for HCs and PD patients. (HC 1 is a 63-year-old male; HC 2 is a 52-year-old female; PD 1 is a 63-year-old male; and PD 2 is a 53-year-old female.).

Table 2
Comparison of NM measurements in the HC and PD groups obtained with PENCIL and MTC.

	Healthy controls	PD patients	P value
NM volume in SNpc-PENCIL (mm^3)	489.4 ± 70.8	303.8 ± 93.0	<0.001
NM volume in SNpc-MTC (mm^3)	454.3 ± 62.8	298.6 ± 76.0	<0.001
CNR- PENCIL	38.0 ± 5.3	36.3 ± 6.5	<0.001
CNR - MTC	31.9 ± 5.6	30.9 ± 7.9	0.557

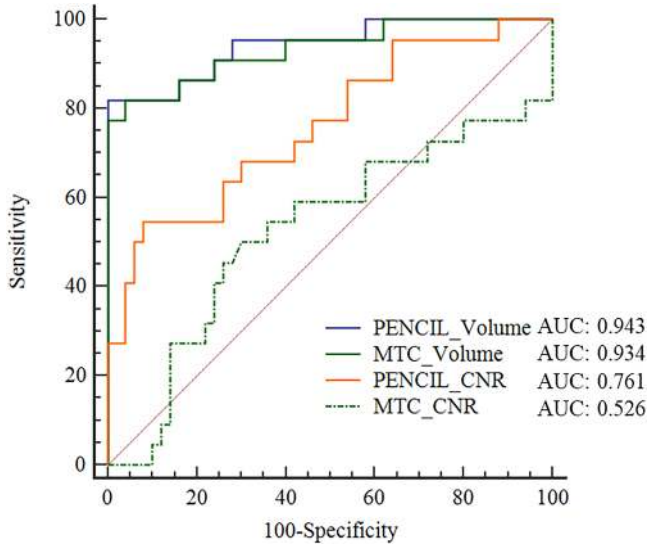

Fig. 3. ROC curves of NM volume in SNpc and CNR analyses for the diagnosis of PD using PENCIL and MTC data.

higher in PENCIL imaging. From the perspective of having a lower bandwidth, the noise was reduced by a factor of 1.34 in PENCIL, leading to an increase in CNR by the same factor. This accounts for the higher CNR observed in PENCIL compared to the MTC approach used in this study.

It has been observed that NM volume in the SNpc can change with age. Our results suggest that the NM volume in SNpc increases up to 50 years of age and then gradually decreases. A previous study (Xing et al., 2018) found a strong increase from childhood to adolescence, with plateauing in middle age and a decline in older age, similar to our findings in the older individuals. This eventual slowdown of NM production and eventual loss may be attributed to the ongoing loss of heavily pigmented neurons with increasing age (Mann et al., 1974). However, these studies are in disagreement with Zecca et al. (2002), who reported a linear increase of NM with age throughout the lifespan.

Because of the improved CNR, the boundary of the SNpc in PENCIL can be delineated more clearly than that in the MTC data and the NM volume in the SNpc measured from PENCIL was significantly higher than that from MTC in HCs. For HCs, the major differences came from the more cranial slices. PENCIL displayed the NM more clearly in these slices (see, for example, the right-hand images in Supplementary Fig. 3). For PD patients, NM in the SNpc has been lost and the differences between the two approaches has been narrowed. NM tends to be brighter in the center of the SNpc for the MTC approach, while it is more uniform using PENCIL. This loss of contrast in some cases could make it hard to delineate the NM in HCs using the usual MTC approach.

Both methods presented decreased NM volume in PD subjects. Numerous studies have shown increased iron content in areas where NM is lost and have demonstrated a reduction in total NM volume in the SNpc among PD subjects (Ghassaban et al., 2019; Biondetti et al., 2020; He et al., 2021, 2023). In summary, it is well known that NM volume in the SNpc plays an important role in the diagnosis of PD. A recent study reported that the AUCs from the ROC analysis of NM volume in the SNpc, total SN volume, SN iron content, and N1 sign were 0.960, 0.788, 0.740, and 0.891, respectively, for PD diagnosis (He et al., 2023). Therefore, it is expected that PENCIL imaging will exhibit equivalent diagnostic performance of NM volume in the SNpc compared with conventional MTC.

There was no significant correlation between UPDRS-III scores and NM volume in SNpc or CNR in our research. The correlation results can be affected by the patients' age, disease severity and disease duration, as well as the method of NM volume measurement and imaging technique. Due to the dopaminergic degeneration, NM signal loss varies regionally within the SN and occurs more at the lateral, posterior, and inferior aspects of the SNpc (Lakhani et al., 2024). Therefore, instead of measuring the whole volume of NM in the SNpc, a voxelwise approach may be more effective to capture this subregional variation (Sulzer et al., 2018; Biondetti et al., 2020). In addition, although the magnitude images using NM-sensitive T1W TSE, MTC GRE, or PDW GRE like PENCIL, can offer good contrast to differentiate PD subjects and HCs, it may not be accurate enough to track NM volume changes over short periods of

time (Sulzer et al., 2018). Our previous research found no correlation between the volume of the SNpc from MTC (SNvol, MTC) and clinical scales, but a significant negative correlation was found between the volume of the SNpc from QSM (SNvol, QSM) and UPDRS-III score (He et al., 2021). However, some previous neuroimaging studies have shown significant correlations of NM volume with either UDPRS-III and/or disease duration (Isaias et al., 2016; Matsuura et al., 2016; Schwarz et al., 2017) while a few other papers were unable to find any clinical correlation with NM volume (Castellanos et al., 2015; Hatano et al., 2017; Schwarz et al., 2017).

The PENCIL technique only requires three minutes for each acquisition with whole brain coverage. That is roughly one minute and thirty seconds faster than the traditional scan which has only coverage of the midbrain. Further, PENCIL with STAGE can provide susceptibility weighted imaging (SWI) and QSM data and a number of other quantitative measures (Wang et al., 2018; Haacke et al., 2020). This makes it possible to evaluate the iron content in the deep gray matter and volumetrics throughout the brain reasonably quickly. In our implementation, we used only a single echo, however, with a slightly longer TR of 22.5 ms, it would be possible to add a second echo of 17.5 ms to allow for the calculation of R2*, an improved susceptibility map and an SWI dataset, providing further insights into brain tissue characteristics. PENCIL can also be used easily at 7T where SAR becomes a more serious problem and would require even longer acquisition times for the MTC sequence.

There are a number of limitations to this study. Firstly, the limited number of cases restricts the generalizability of the ROC calculations. Further studies on a larger cohort of PD subjects should be performed to demonstrate its reliability for clinical utility. Secondly, even though the low FA of 3° effectively visualizes the NM in the SN, it may not provide optimal contrast for visualizing the LC. Leveraging the capabilities of STAGE imaging could allow for the simulation of higher FAs as mentioned above, which would be more suitable for visualizing the LC (Liu et al., 2020, Supplementary Fig. 6).

In conclusion, we have proposed a new PENCIL imaging approach to map NM in the midbrain. PENCIL has comparable performance to the conventional MTC approach in terms of measuring NM volume in the SNpc, CNR and the ability to differentiate PD patients from healthy controls. A major advantage of PENCIL is the rapid whole-brain coverage compared to the limited coverage with MTC.

Data and code availability statement

The data supporting the reported findings are available from the corresponding author upon reasonable request.

Funding sources for study

This work was supported by the National Natural Science Foundation of China (grant numbers: 82271954 and 81971576 for Fuhua Yan, MD, PhD.), National Key R&D Program of China (2022YFC2009900/2022YFC2009905) and the Innovative Research Team of High-level Local Universities in Shanghai.

CRediT authorship contribution statement

Peng Liu: Writing – original draft, Data curation, Investigation, Formal analysis, Visualization. **Xinhui Wang:** Writing – original draft, Writing – review & editing, Investigation, Formal analysis. **Youmin Zhang:** Writing – review & editing, Writing – original draft, Investigation. **Pei Huang:** Writing – review & editing, Investigation. **Zhijia Jin:** Writing – review & editing, Investigation. **Zenghui Cheng:** Writing – review & editing, Investigation. **Yongsheng Chen:** Writing – review & editing, Formal analysis. **Qiuyun Xu:** Writing – review & editing, Formal analysis. **Kiarash Ghassaban:** Writing – review & editing, Formal analysis. **Yu Liu:** Writing – review & editing, Investigation. **Shengdi Chen:** Resources, Supervision. **Naying He:** Conceptualization, Supervision, Funding acquisition, Resources, Writing – review & editing. **Fuhua Yan:** Conceptualization, Supervision, Funding acquisition, Resources, Writing – review & editing. **E. Mark Haacke:** Conceptualization, Supervision, Resources, Writing – review & editing.

Declaration of competing interest

None.

Data availability

Data will be made available on request.

Supplementary materials

Supplementary material associated with this article can be found, in the online version, at doi:10.1016/j.neuroimage.2024.120588.

References

Biondetti, E., Gaurav, R., Yahia-Cherif, L., Mangone, G., Pyatigorskaya, N., Valabrègue, R., Ewenczyk, C., Hutchison, M., François, C., Arnulf, I., Corvol, J.C., Vidailhet, M., Lehéricy, S., 2020. Spatiotemporal changes in substantia nigra neuromelanin content in Parkinson's disease. Brain 143, 2757–2770. https://doi.org/10.1093/brain/awaa216.

Chen, Y., Liu, S., Wang, Y., Kang, Y., Haacke, E.M., 2018. STrategically acquired gradient echo (STAGE) imaging, part I: creating enhanced T1 contrast and standardized susceptibility weighted imaging and quantitative susceptibility mapping. Magn. Reson. ImAging 46, 130–139. https://doi.org/10.1016/j.mri.2017.10.005.

Damier, P., 1999. The substantia nigra of the human brain. II. Patterns of loss of dopamine-containing neurons in Parkinson's disease. Brain 122, 1437–1448. https://doi.org/10.1093/brain/122.8.1437.

Fabbri, M., Reimão, S., Carvalho, M., Nunes, R.G., Abreu, D., Guedes, L.C., Bouça, R., Lobo, P.P., Godinho, C., Coelho, M., Gonçalves, N.C., Rosa, M.M., Antonini, A., Ferreira, J.J., 2017. Substantia nigra neuromelanin as an imaging biomarker of disease progression in Parkinson's disease. J. Parkinsons Dis. 7, 491–501. https://doi.org/10.3233/JPD-171135.

Castellanos, G., Fernández-Seara, M.A., Lorenzo-Betancor, O., Ortega-Cubero, S., Puigvert, M., Uranga, J., Vidorreta, M., Irigoyen, J., Lorenzo, E., Muñoz-Barrutia, A., Ortiz-de-Solorzano, C., Pastor, P., Pastor, M.A., 2015. Automated neuromelanin imaging as a diagnostic biomarker for Parkinson's disease. Mov. Disord. 30, 945–952. https://doi.org/10.1002/mds.26201.

Goetz, C.G., Tilley, B.C., Shaftman, S.R., Stebbins, G.T., Fahn, S., Martinez-Martin, P., Poewe, W., Sampaio, C., Stern, M.B., Dodel, R., Dubois, B., Holloway, R., Jankovic, J., Kulisevsky, J., Lang, A.E., Lees, A., Leurgans, S., LeWitt, P.A., Nyenhuis, D., Olanow, C.W., Rascol, O., Schrag, A., Teresi, J.A., van Hilten, J.J., LaPelle, N., 2008. Movement disorder society UPDRS revision task force. Movement disorder society-sponsored revision of the unified Parkinson's disease rating scale (MDS-UPDRS): scale presentation and clinimetric testing results. Mov. Disord. 23, 2129–2170. https://doi.org/10.1002/mds.22340.

Gaurav, R., Yahia-Cherif, L., Pyatigorskaya, N., Mangone, G., Biondetti, E., Valabrègue, R., Ewenczyk, C., Hutchison, R.M., Cedarbaum, J.M., Corvol, J.C., Vidailhet, M., Lehéricy, S., 2021. Longitudinal changes in neuromelanin MRI signal in parkinson's disease: a progression marker. Mov. Disord. 36, 1592–1602. https://doi.org/10.1002/mds.28531.

Hatano, T., Okuzumi, A., Kamagata, K., Daida, K., Taniguchi, D., Hori, M., Yoshino, H., Aoki, S., Hattori, N., 2017. Neuromelanin MRI is useful for monitoring motor complications in Parkinson's and PARK2 disease. J. Neural Transm. 124, 407–415. https://doi.org/10.1007/s00702-017-1688-9 (Vienna).

Haacke, E.M., Chen, Y., Utriainen, D., Wu, B., Wang, Y., Xia, S., He, N., Zhang, C., Wang, X., Lagana, M.M., Luo, Y., Fatemi, A., Liu, S., Gharabaghi, S., Wu, D., Sethi, S. K., Huang, F., Sun, T., Qu, F., Yadav, B.K., Ma, X., Bai, Y., Wang, M., Cheng, J., Yan, F., 2020. STrategically acquired Gradient Echo (STAGE) imaging, part III: technical advances and clinical applications of a rapid multi-contrast multi-parametric brain imaging method. Magn. Reson. ImAging 65, 15–26. https://doi.org/10.1016/j.mri.2019.09.006.

He, N., Ghassaban, K., Huang, P., Jokar, M., Wang, Y., Cheng, Z., Jin, Z., Li, Y., Sethi, S. K., He, Y., Chen, Y., Gharabaghi, S., Chen, S., Yan, F., Haacke, E.M, 2021. Imaging iron and neuromelanin simultaneously using a single 3D gradient echo magnetization transfer sequence: combining neuromelanin, iron and the nigrosome-1 sign as complementary imaging biomarkers in early stage Parkinson's disease. Neuroimage 230, 117810. https://doi.org/10.1016/j.neuroimage.2021.117810.

He, N., Chen, Y., LeWitt, P.A., Yan, F., Haacke, E.M., 2023. Application of neuromelanin MR imaging in Parkinson disease. J. Magn. Reson. Imaging 57, 337–352. https://doi.org/10.1002/jmri.28414.

Isaias, I.U., Trujillo, P., Summers, P., Marotta, G., Mainardi, L., Pezzoli, G., Zecca, L., Costa, A., 2016. Neuromelanin imaging and dopaminergic loss in Parkinson's disease. Front. Aging Neurosci. 22, 196. https://doi.org/10.3389/fnagi.2016.00196.

Jin, Z., Wang, Y., Jokar, M., Li, Y., Cheng, Z., Liu, Y., Tang, R., Shi, X., Zhang, Y., Min, J., Liu, F., He, N., Yan, F., Haacke, E.M., 2022. Automatic detection of neuromelanin and iron in the midbrain nuclei using a magnetic resonance imaging-based brain template. Hum. Brain Mapp. 43, 2011–2025. https://doi.org/10.1002/hbm.25770.

Jokar, M., Jin, Z., Huang, P., Wang, Y., Zhang, Y., Li, Y., Cheng, Z., Liu, Y., Tang, R., Shi, X., Min, J., Liu, F., Chen, S., He, N., Haacke, E.M., Yan, F., 2023. Diagnosing Parkinson's disease by combining neuromelanin and iron imaging features using an automated midbrain template approach. Neuroimage 266, 119814. https://doi.org/10.1016/j.neuroimage.2022.119814.

Keren, N.I., Lozar, C.T., Harris, K.C., Morgan, P.S., Eckert, M.A., 2009. In vivo mapping of the human locus coeruleus. Neuroimage 47, 1261–1267. https://doi.org/10.1016/j.neuroimage.2009.06.012.

Matsuura, K., Maeda, M., Tabei, K.I., Umino, M., Kajikawa, H., Satoh, M., Kida, H., Tomimoto, H., 2016. A longitudinal study of neuromelanin-sensitive magnetic resonance imaging in Parkinson's disease. Neurosci. Lett. 28, 112–117. https://doi.org/10.1016/j.neulet.2016.09.011.

Ghassaban, K., Liu, S., Jiang, C., Haacke, E.M., 2019. Quantifying iron content in magnetic resonance imaging. Neuroimage 15, 77–92. https://doi.org/10.1016/j.neuroimage.2018.04.047.

Lakhani, D.A., Zhou, X., Tao, S., Patel, V., Wen, S., Okromelidze, L., Greco, E., Lin, C., Westerhold, E.M., Straub, S., Wszolek, Z.K., Tipton, P.W., Uitti, R.J., Grewal, S.S., Middlebrooks, E.H., 2024. Diagnostic utility of 7T neuromelanin imaging of the substantia nigra in Parkinson's disease. NPJ. Parkinsons Dis. 10, 13. https://doi.org/10.1038/s41531-024-00631-3.

Lotankar, S., Prabhavalkar, K.S., Bhatt, L.K., 2017. Biomarkers for Parkinson's disease: recent advancement. Neurosci. Bull. 33, 585–597. https://doi.org/10.1007/s12264-017-0183-5.

Liu, Y., Li, J., He, N., Chen, Y., Jin, Z., Yan, F., Haacke, E.M., 2020. Optimizing neuromelanin contrast in the substantia nigra and locus coeruleus using a magnetization transfer contrast prepared 3D gradient recalled echo sequence. Neuroimage 218, 116935. https://doi.org/10.1016/j.neuroimage.2020.116935.

Mann, D.M., Yates, P.O., 1974. Lipoprotein pigments–their relationship to ageing in the human nervous system. II. The melanin content of pigmented nerve cells. Brain 97, 489–498. https://doi.org/10.1093/brain/97.1.489.

Nakane, T., Nihashi, T., Kawai, H., Naganawa, S., 2008. Visualization of neuromelanin in the Substantia nigra and locus ceruleus at 1.5T using a 3D-gradient echo sequence with magnetization transfer contrast. Magn. Reson. Med. Sci. 7, 205–210. https://doi.org/10.2463/mrms.7.205.

Oshima, S., Fushimi, Y., Okada, T., Nakajima, S., Yokota, Y., Shima, A., Grinstead, J., Ahn, S., Sawamoto, N., Takahashi, R., Nakamoto, Y., 2021. Neuromelanin-sensitive magnetic resonance imaging using DANTE pulse. Mov. Disord. 36, 874–882. https://doi.org/10.1002/mds.28417.

Postuma, R.B., Berg, D., Stern, M., Poewe, W., Olanow, C.W., Oertel, W., Obeso, J., Marek, K., Litvan, I., Lang, A.E., Halliday, G., Goetz, C.G., Gasser, T., Dubois, B., Chan, P., Bloem, B.R., Adler, C.H., Deuschl, G., 2015. MDS clinical diagnostic criteria for Parkinson's disease. Mov. Disord. 30, 1591–1601. https://doi.org/10.1002/mds.26424.

Prasad, S., Stezin, A., Lenka, A., George, L., Saini, J., Yadav, R., Pal, P.K., 2018. Three-dimensional neuromelanin-sensitive magnetic resonance imaging of the substantia nigra in Parkinson's disease. Eur. J. Neurol. 25, 680–686. https://doi.org/10.1111/ene.13573.

Priovoulos, N., Jacobs, H.I.L., Ivanov, D., Uludağ, K., Verhey, F.R.J., Poser, B.A., 2018. High-resolution in vivo imaging of human locus coeruleus by magnetization transfer MRI at 3T and 7T. Neuroimage 168, 427–436. https://doi.org/10.1016/j.neuroimage.2017.07.045.

Sasaki, M., Shibata, E., Tohyama, K., Takahashi, J., Otsuka, K., Tsuchiya, K., Takahashi, S., Ehara, S., Terayama, Y., Sakai, A., 2006. Neuromelanin magnetic resonance imaging of locus ceruleus and substantia nigra in Parkinson's disease. Neuroreport 17, 1215–1218. https://doi.org/10.1097/01.wnr.0000227984.84927.a7.

Schwarz, S.T., Xing, Y., Tomar, P., Bajaj, N., Auer, D.P., 2017. In vivo assessment of brainstem depigmentation in Parkinson disease: potential as a severity marker for multicenter studies. Radiology 283, 789–798. https://doi.org/10.1148/radiol.2016160662.

Sulzer, D., Cassidy, C., Horga, G., Kang, U.J., Fahn, S., Casella, L., Pezzoli, G., Langley, J., Hu, X.P., Zucca, F.A., Isaias, I.U., Zecca, L., 2018. Neuromelanin detection by magnetic resonance imaging (MRI) and its promise as a biomarker for Parkinson's disease. NPJ Parkinsons Dis. 10, 11. https://doi.org/10.1038/s41531-018-0047-3.

Trujillo, P., Summers, P.E., Ferrari, E., Zucca, F.A., Sturini, M., Mainardi, L.T., Cerutti, S., Smith, A.K., Smith, S.A., Zecca, L., Costa, A., 2017a. Contrast mechanisms associated with neuromelanin-MRI. Magn. Reson. Med. 78, 1790–1800. https://doi.org/10.1002/mrm.26584.

Trujillo, P., Summers, P.E., Smith, A.K., Smith, S.A., Mainardi, L.T., Cerutti, S., Claassen, D.O., Costa, A., 2017b. Pool size ratio of the substantia nigra in Parkinson's disease derived from two different quantitative magnetization transfer approaches. Neuroradiology 59, 1251–1263. https://doi.org/10.1007/s00234-017-1911-2.

Takahashi, H., Watanabe, Y., Tanaka, H., Mihara, M., Mochizuki, H., Liu, T., Wang, Y., Tomiyama, N., 2018. Quantifying changes in nigrosomes using quantitative susceptibility mapping and neuromelanin imaging for the diagnosis of early-stage Parkinson's disease. Br. J. Radiol. 91, 20180037 https://doi.org/10.1259/bjr.20180037.

Trujillo, P., Petersen, K.J., Cronin, M.J., Lin, Y.C., Kang, H., Donahue, M.J., Smith, S.A., Claassen, D.O., 2019. Quantitative magnetization transfer imaging of the human locus coeruleus. Neuroimage 200, 191–198. https://doi.org/10.1016/j.neuroimage.2019.06.049.

Wang, Y., Chen, Y., Wu, D., Wang, Y., Sethi, S.K., Yang, G., Xie, H., Xia, S., Haacke, E.M., 2018. STrategically acquired gradient echo (STAGE) imaging, part II: correcting for RF inhomogeneities in estimating T1 and proton density. Magn. Reson. ImAging 46, 140–150. https://doi.org/10.1016/j.mri.2017.10.006.

Watanabe, T., Tan, Z., Wang, X., Martinez-Hernandez, A., Frahm, J., 2019. Magnetic resonance imaging of noradrenergic neurons. Brain Struct. Funct. 224, 1609–1625. https://doi.org/10.1007/s00429-019-01858-0.

Wang, L., Yan, Y., Zhang, L., Liu, Y., Luo, R., Chang, Y., 2021. Substantia nigra neuromelanin magnetic resonance imaging in patients with different subtypes of Parkinson disease. J. Neural Transm. 128, 171–179. https://doi.org/10.1007/s00702-020-02295-8 (Vienna).

Xing, Y., Sapuan, A., Dineen, R.A., Auer, D.P., 2018. Life span pigmentation changes of the substantia nigra detected by neuromelanin-sensitive MRI. Mov. Disord. 33, 1792–1799. https://doi.org/10.1002/mds.27502.

Zecca, L., Fariello, R., Riederer, P., Sulzer, D., Gatti, A., Tampellini, D., 2002. The absolute concentration of nigral neuromelanin, assayed by a new sensitive method, increases throughout the life and is dramatically decreased in Parkinson's disease. FEBS Lett. 510, 216–220. https://doi.org/10.1016/s0014-5793(01)03269-0.